ELSEVIER

J. Non-Newtonian Fluid Mech., 66 (1996) 127–144

Journal of Non-Newtonian Fluid Mechanics

Non-Newtonian shear-thinning flows past a flat plate

J. Wu[a], M.C. Thompson[b,*]

[a]*CSIRO Division of Building, Construction and Engineering, P.O. Box 56, Highett Vict. 3190, Australia*
[b]*Department of Mechanical Engineering, Monash University, Clayton, Vict. 3168, Australia*

Received 15 March 1995; in revised form 1 May 1996

Abstract

The present work attempts to characterize the flow of shear-thinning power-law fluids past a flat plate as the angle of attack is varied. The effects of Reynolds number, shear-thinning characteristics and angles of attack on drag and lift of the flat plate were investigated, both experimentally and numerically. Carbopol 940 solutions of various strengths were used to approximate purely viscous shear-thinning non-Newtonian fluids for the experiments. An important finding is that at small angles of attack when the wall shear forms the dominant contribution to the drag, the non-Newtonian shear-thinning property leads to drag reduction, whereas for large angles of attack, when pressure-induced form drag is dominant, shear-thinning results in drag augmentation. This is consistent with the trend shown in the present study that lift increases as shear-thinning increases. It is demonstrated that a simple linear model developed for Newtonian creeping flow can be used to estimate the effect of angle on drag given both the drag coefficients corresponding to normal and tangential flow to the plate.

Keywords: Non-newtonians; Shear-thinning flows

1. Introduction

The present study is concerned with flat-plate flows of shear-thinning fluids which obey a simple power-law stress–strain relationship. The study stems from a desire to understand non-Newtonian flows around agitator impellers in mixing vessels, where skin friction and pressure distributions are directly related to the pumping rate and power consumption of the impellers. As a first step in achieving this aim, the drag and lift of a two-dimensional flat plate at an arbitrary angle of attack were determined for both Newtonian and non-Newtonian shear-thinning fluids.

* Corresponding author.

0377-0257/96/$15.00 Copyright © 1996 Elsevier Science B.V. All rights reserved.
PII S0377-0257(96)01476-0

There are numerous experimental and computational studies on drag of spherical bodies in non-Newtonian fluid flows (e.g. [1–4], to mention just a few). A considerable body of information on the motion of rigid spherical particles falling in incompressible Newtonian or non-Newtonian fluid media has been summarized by Chhabra [5]. Estimation of the drag coefficient of particles has been made possible, given the fact that a wealth of experimental correlations of drag with Reynolds number, rheological properties and wall effects are available.

In comparison, much less work has been done for non-spherical bodies, even for those of a regular shape such as cylinders and plates. The main concern of the present work is flow past a flat plate where the corresponding literature is very sparse. Most of the investigations found in the literature consider the flow past a flat plate placed tangential to the flow with infinite plate length, which is a special case of the present study. The drag in this case is associated with boundary layer developement, which generally has been treated by Prandtl's boundary layer approximation. Representative works using boundary layer theory can be found in the early papers by Schowalter [6] and Acrivos et al. [7] and also more recently by Nakayama [8] and Andersson and Toften [9]. However, since high viscosity (or equivalently low Reynolds number) is often the case for non-Newtonian fluid flows, the errors resulting from applying boundary layer theory can be substantial and experimental or computational validation, which is often lacking, is particularly needed. This is part of the objective of the present paper.

In et al. [10] solved Newtonian flow past a flat plate at various angles of incidence numerically for Reynolds numbers up to 30. Their simulations show that the flow develops into patterns of two-vortex, one-vortex or no-vortex regions depending on Reynolds number and angle of incidence. It can also be concluded from their results that lift and drag coefficients decrease as the Reynolds number increases. No comparison with experiments, however, was mentioned in their work. Another relevant study was performed by Tamada et al. [11], again only for Newtonian fluids. They showed that for small Reynolds numbers, the asymptotic flow field at large distances from an immersed body is dependent on the force acting on the body. This enabled them to evaluate the force acting on the body as a function of the flow Reynolds number. Their calculations provided the drag coefficient variation with Reynolds number for a flat plate orientated either tangentially or normally to the flow at small Reynolds numbers.

Published experimental data for drag and lift are not available in the low Reynolds number range for a flat plate as a function of angle of attack. This lack of information also exists for non-Newtonian fluids. The objective of the present work is to address this lack of knowledge and is aimed at providing detailed force coefficient data. Experimental results obtained using a force balance device in a closed-circuit liquid tunnel and computational results obtained using a finite-element code will be presented. The philosophy of the present approach of using both experimental and computational methods is that the latter, once validated by the former at each stage of investigation, can be used to explore the influence of various parameters rapidly and reliably with minimum effort.

This study covers Reynolds numbers ranging from $Re < 1$ (creeping flow range) to an intermediate region ($Re \approx 200$) where the Reynolds number is sufficiently high that both inertia and viscous forces are important. The power-law model is considered in order to investigate the influence of shear-thinning rheological properties on both drag and lift coefficients.

2. Experimental facilities

2.1. Test tunnel

A return-circuit liquid test tunnel located at CSIRO, Highett, Australia, was used for the experiments, as shown schematically in Fig. 1. The working section of the tunnel is 770 mm long, 244 mm wide and 244 mm high, and the walls are made of transparent acrylic material. The velocity of the tunnel can be varied using a variable speed controller and the maximum velocity in the working section is approximately 0.4 m s^{-1}. Flat plates 20, 40, 59

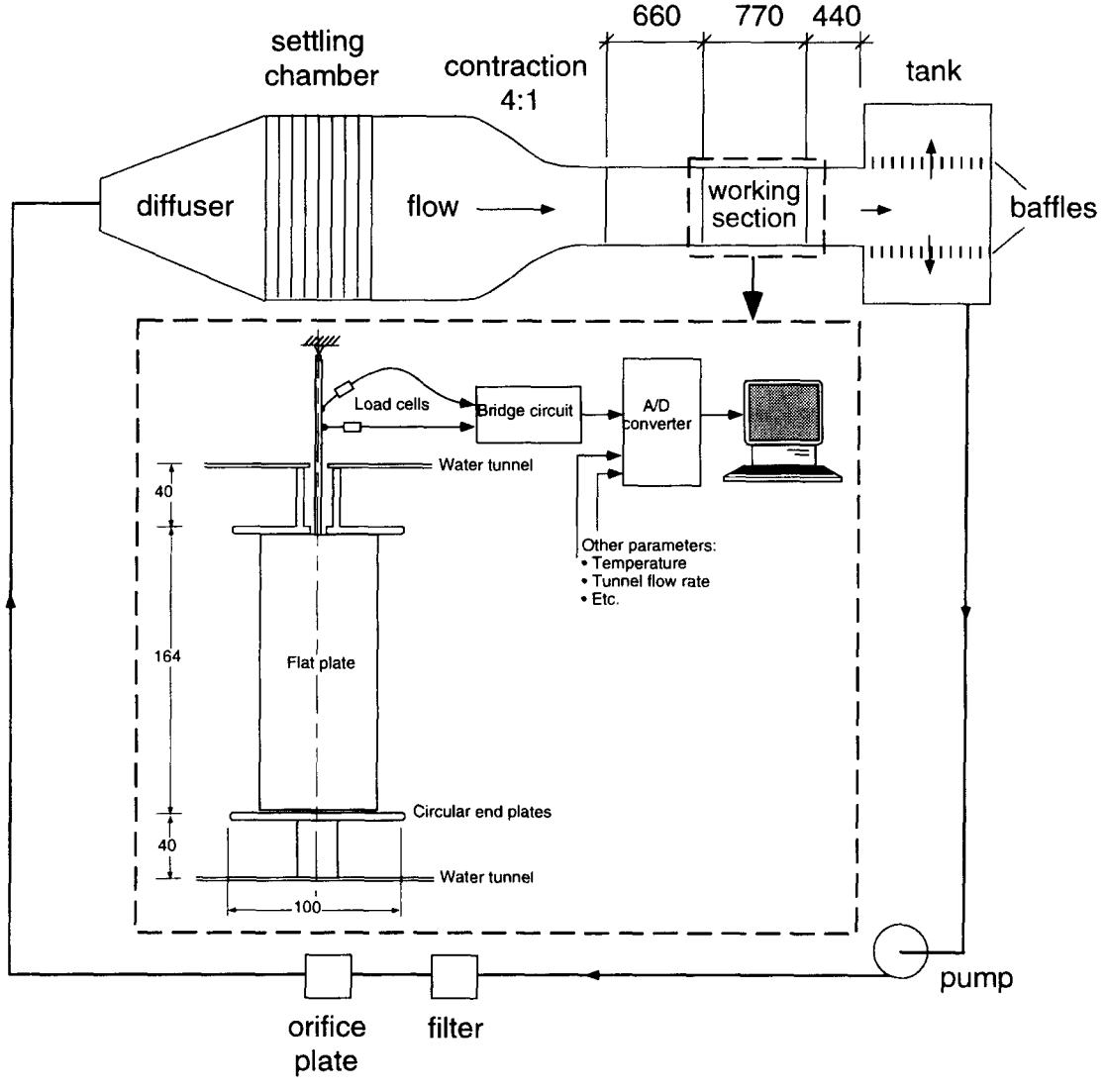

Fig. 1. Closed-circuit test tunnel and the force measurement system.

and 70 mm in length, all with a thickness of 1.6 mm, were used for the experiments. Two circular endplates were employed to minimize tunnel boundary layer interference.

2.2. Force measurement

The force balance measurement system is also shown schematically in Fig. 1. The flat plate section under test was connected to a pendulum-type force amplification balance mounted on a universal joint. Two load cells manufactured by Transducer Technology were used to measure drag and lift of the plate simultaneously. The load cell were interfaced to an analogue to digital (A/D) data acquisition system in an IBM-compatible 486PC. Calibration of the force measurement system was conducted using known weights suspended from cord lines over pulleys. The error in the force measurement was estimated by comparing computer readings based on calibration coefficients and known weights. It was found that the system had an uncertainty of 0.2 g at the 95% confidence level. Typically, this corresponds to a full-scale system error of 0.4% at the 95% confidence level.

2.3. Test fluid

The test fluid consisted of a clear, neutralized aqueous solution of Carbopol 940. A volume of 1000 l was pumped around the test tunnel. The concentrations used were 0.125, 0.09 and 0.05% by weight. The fluid exhibits shear-thinning characteristics, i.e. the viscosity of the liquid reduces as shear rate increases. The apparent viscosity of the fluid was measured using a Contraves Rheomat 108 and a Carri-med CSL100 cone and plate rheometer. Brookfield viscosity standards were used to validate rheological measurements.

Fig. 2 shows the apparent viscosity of the Carbopol solutions. Carbopol fluid is known to possess a yield stress, however, within the range of shear rate of interest a power-law relationship was found to characterize adequately the viscosity versus shear-rate behaviour. This was implied by the linear variation shown in the log–log plot in Fig. 2 The equation for the power-law model is

$$\tau = K\dot{\gamma}^n, \tag{1}$$

where n is a non-dimensional power-law index and K is a consistency parameter. Typical values for n and K used in the present experiments are listed in Table 1.

A slow viscosity degradation was observed which was attributed to the shearing experienced by the circulation of the fluid in the tunnel and rheological measurements were conducted before and after each experiment. The viscosity of the liquid is also sensitive to temperature and consequently the latter was monitored to ensure that it was maintained within the range 16.5 ± 0.5°C.

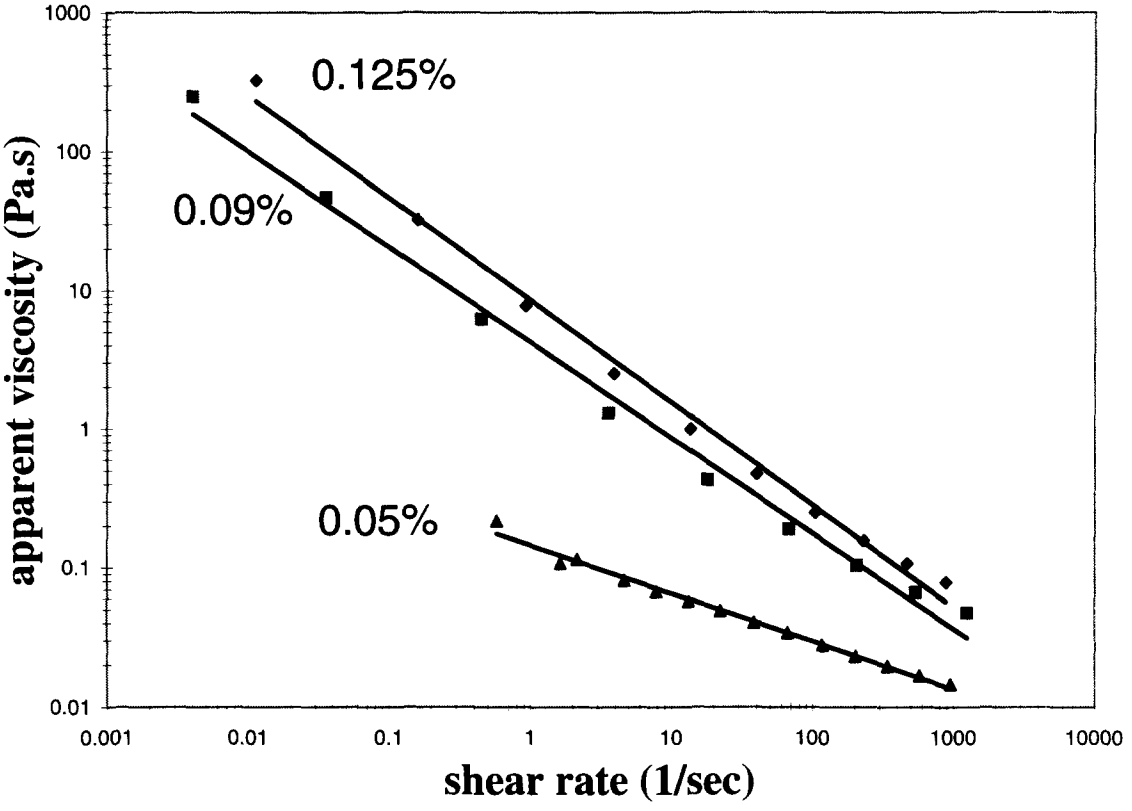

Fig. 2. Rheology of Carbopol 940 water solution over a range of concentration.

3. Theory and numerical method

3.1. Newtonian creeping flow: a linear model

In order to understand the flow at low Reynolds numbers, it is illuminating to examine the extreme case, i.e. creeping flow. For Newtonian creeping flow ($\mathrm{Re} \ll 1$), the inertia force is negligible and the Navier–Stokes equations simplify to

$$\frac{\nabla p}{\rho} - \mu \nabla \boldsymbol{u} = 0, \tag{2}$$

Table 1
Typical parameters used in the experiments

Fluids	n	K ($Pa\ s^n$)	Shear rate (s^{-1})
0.125% Carbopol	0.32	6.67	1–100
0.09% Carbopol	0.44	2.37	1–100
0.05% Carbopol	0.65	0.1103	1–100

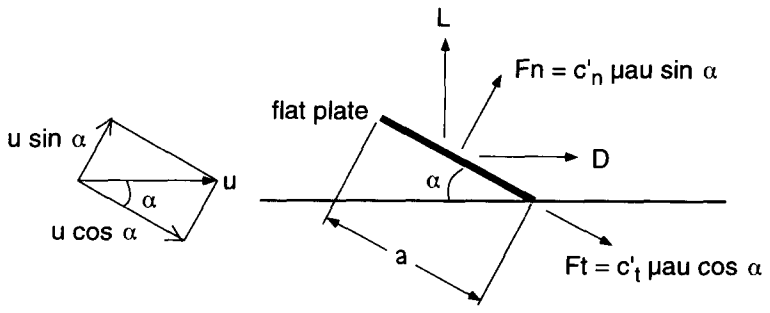

Fig. 3. Resultant force acting on a flat plate for creeping Newtonian flow using the linear superposition model.

where p is the pressure, ρ is the density, μ is the viscosity and $\boldsymbol{u}$ is the velocity vector. Since this equation is linear, a linear superposition of solutions can be applied to predict the resultant force on a flat plate placed at an angle to the incoming flow, denoted by α, as shown schematically in Fig. 3. The velocity vector is decomposed into a tangential component, $u_t = u \cos \alpha$ and a normal component $u_n = u \sin \alpha$. The forces associated with the two velocity components are F_t and F_n, respectively. They correspond to the drag force of the plate at $\alpha = 0$ and $\alpha = 90$.

Assuming the Stokes drag equation is applicable and the flat plate has a unit width:

$$F_t = C'_t \mu a u \cos \alpha, \tag{3}$$

$$F_n = C'_n \mu a u \sin \alpha, \tag{4}$$

where C'_t and C'_n are constants dependent on plate geometry but independent of velocity, and a is the plate length. The lift force L can be expressed as

$$L = F_n \cos \alpha - F_t \sin \alpha$$

$$= \frac{\mu a u}{2} (C'_n - C'_t) \sin 2\alpha, \tag{4}$$

and similarly the drag D can be written:

$$D = F_n \sin \alpha + F_t \cos \alpha$$

$$= \mu a u (C'_n \sin^2 \alpha + C'_t \cos^2 \alpha). \tag{5}$$

A consequence of the above formulation is that in the Newtonian creeping flow region, the drag or lift of a flat plate at an arbitrary angle of attack can be evaluated using only the normal and tangential drag coefficients.

Although these equations are developed for Newtonian creeping flow, it will be shown later than experimental results suggest that they can be used to estimate the flat plate drag to a good degree of accuracy for non-Newtonian shear-thinning flows over a wide range of Reynolds numbers.

3.2. Numerical technique

The time-independent Navier–Stokes equations can be written as

$$\rho(\boldsymbol{u}\cdot\nabla)\boldsymbol{u} = -\nabla p + \nabla\cdot\tau$$

and

$$\nabla\cdot\boldsymbol{u} = 0,$$

where τ is the stress tensor. For a shear-thinning fluid, the shear stress can be expressed in the form

$$\tau = 2\eta(\dot{\gamma})\boldsymbol{S}.$$

The cartesian components of the rate of strain tensor ($\boldsymbol{S}$) are given by

$$S_{ij} = \frac{1}{2}\left(\frac{\partial u_i}{\partial x_j} + \frac{\partial u_j}{\partial x_i}\right),$$

and η is the viscosity which in general depends on the shear rate, $\dot{\gamma} = \sqrt{2\Sigma_{ij}(S_{ij}S_{ij})}$.

The rheological relationship between viscosity and shear rate under investigation in this paper is of the form

$$\eta = K\dot{\gamma}^{n-1}. \tag{6}$$

For the calculations described in this paper, the two-dimensional Navier–Stokes equations are discretized using the Galerkin finite-element method (FEM). The penalty function approach is used to eliminate explicitly the pressure from the computations by penalizing the continuity constraint. Explicitly, the pressure is expressed as

$$p = -\lambda\rho\nabla\cdot\boldsymbol{u},$$

where λ is a large parameter which can depend on the Reynolds number. For the range of Re under investigation, typically it is taken as 10^6; however, the results are not sensitive to the exact value. The method is standard and details can be found in Zienkiewicz and Taylor [12], for example.

The discretized non-linear equations formed from the application of the Galerkin finite-element method are solved by the generalized Newton method. The dependence of the viscosity on the shear-rate is explicitly taken into account in the formation of the Jacobian matrix leading to quadratic convergence of the iteration process. However, since the radius of convergence of Newton's method is generally small, the solution is approached gradually by either or both, starting from a lower Reynolds number solution, or from a fluid with weaker shear-thinning behaviour. For the Reynolds number range investigated, achieving convergence was not difficult.

The code was validated by comparing predictions for a test problem described by Rubart and Böhme [13]. In particular, the anchor and blade impeller problem that they described was set up and solved. The resulting predictions of the stream function at the wall of the vessel agreed to within approximately 0.1% over the ranges of shear-thinning parameters and Reynolds numbers studied.

4. Results

4.1. Experimental validation of FEM code

The drag coefficient is defined as $C_D = D/(1/2\rho U^2)a$, where D is drag, U is free stream velocity, a is plate length and ρ is density. In general, C_D is a function of α, the angle of attack, i.e. $C_D = C_D(\alpha)$. The drag coefficients at $\alpha = 0°$ and 90° are of some special interest and are denoted by C_{Dt} and C_{Dn} for later use (i.e. $C_{Dt} = C_D(0)$ and $C_{Dn} = C_D(90)$). The generalized plate Reynolds number is defined, using power-law model parameters, as

$$\mathrm{Re} = \frac{\rho U^{2-n} a^n}{K}. \tag{7}$$

Fig. 4 shows a comparison of experimental results and FEM simulations for $n = 0.32$. For the plate placed tangentially to flow, drag of two different plate lengths were measured to show that the data collapsed on to a single line. In general, it can be concluded that the experimental and computed results are in good agreement, except for the case of the flat plate placed normally to the flow or at low Reynolds numbers, where the experimental results predict a higher value. The

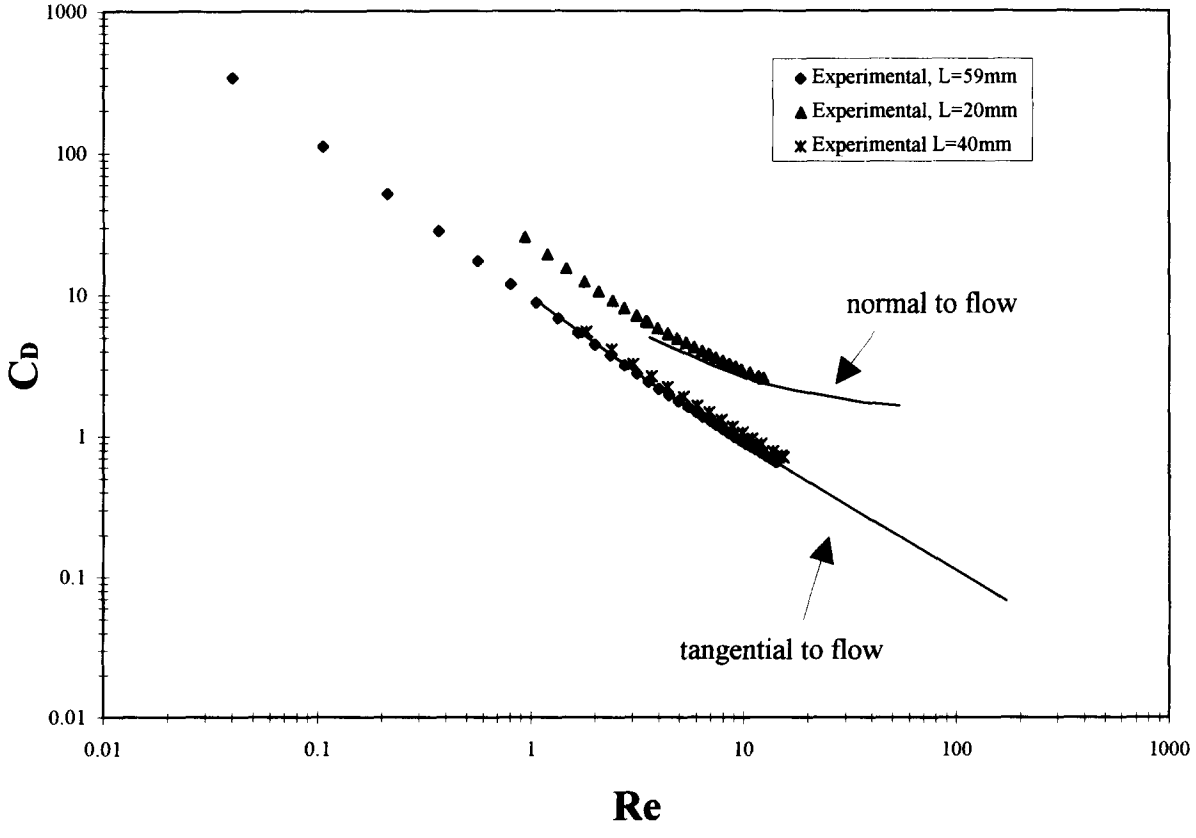

Fig. 4. Experimental validation of the FEM code, shear-thinning index $n = 0.32$.

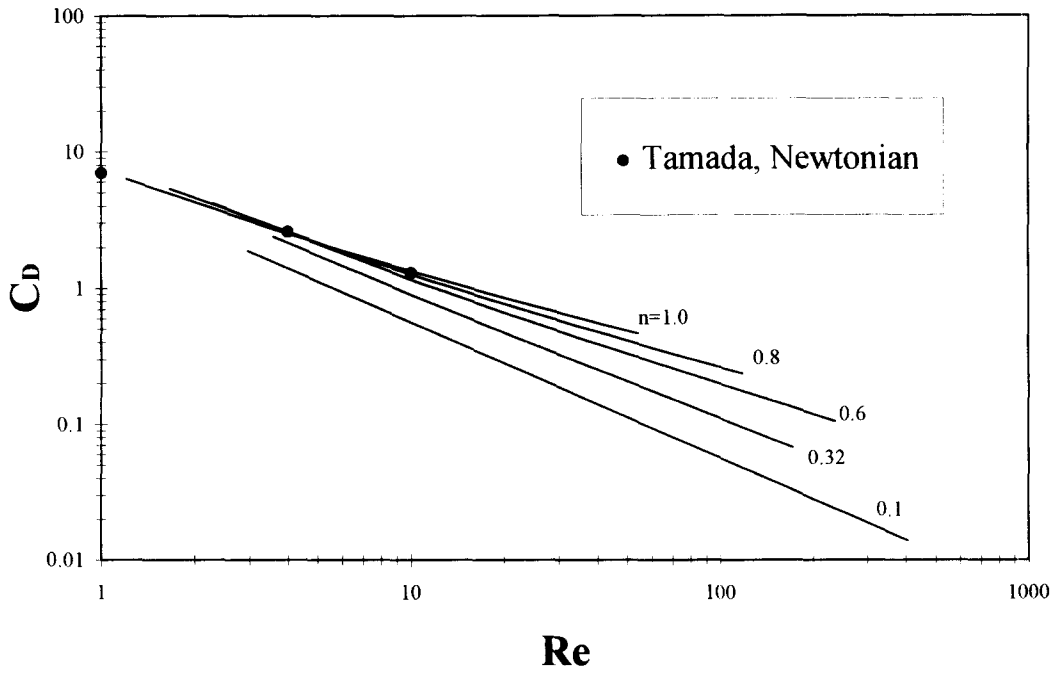

Fig. 5. Drag coefficient of a flat plate placed tangentially to Newtonian and non-Newtonian flows.

discrepancy is probably a result of water tunnel blockage, which is most severe for the normal flow case. Support for this hypothesis was obtained by measuring the drag for different plate lengths (and thus an increase in blockage) leads to an increase in drag coefficient.

4.2. *Flat plate tangential to the flow*

Fig. 5 summarizes the results of the FEM simulations for a range of power-law index n on a logarithmic scale. Also included are the numerical results of Tamada et al. [11] for Newtonian flow, showing good agreement. In the low Reynolds number region, i.e. $Re = 1-10$, the variation of drag coefficient with shear thinning index is not significant. At higher Reynolds numbers, there is a strong dependence of C_D on n. For a given Re, a reduction in n, corresponding to an increase in the non-Newtonian shear-thinning effect, results in a decrease in C_D. This drag reduction behaviour is similar to that found for shear-thinning flow past spheres, as reported by many authors. Amongst others, Mena and Manero [4] measured the drag force acting on a sphere moving inside a container using a balance device. They found that the drag reduction for both shear-thinning inelastic Carbopol fluid and elastic Boger fluid is large.

Traditionally, this flow has been considered in the context of boundary layer development. Using boundary layer theory, Acrivos et al. [7] showed that the wall shear stress can be represented by

$$\frac{\tau_0}{\rho U^2} = (\mathrm{Re}_x)^{-1/(1+n)} C(n), \tag{8}$$

where Re_x is the generalized Reynolds number for power-law fluids based on x, the distance from the leading edge of the plate and the external velocity U, τ_0 is the wall shear stress, ρ is the fluid density and $C(n)$ is a function dependent on n, the power-law index. One objective of the present work is to estimate the error resulting from applying boundary layer theory at lower Reynolds numbers, for which the accuracy of the boundary layer assumptions is questionable. This will allow the minimum Reynolds number to be determined for which boundary layer theory provides reasonable accuracy as a function of shear-thinning index.

Fig. 6(a)–(c) show the wall shear stress distributions at three Reynolds numbers for $n = 0.28$, where x is the coordinate measured from the plate leading edge. The prediction using the boundary layer approximations of Eq. (8) are included for comparison. Not surprisingly, the discrepancy between the FEM results and boundary layer predictions is large for lower Reynolds number. For example, at $Re = 3.9$, the boundary layer prediction underestimates the shear stress by about 50% over almost the entire length of the plate.

As the Reynolds number increases the agreement improves. Reasonable agreement over the firs half of the plate is observed for $Re = 42.7$; however, the discrepancy is still large for the trailing-edge section. As the Reynolds number is further increased to 86.5, the FEM and boundary layer predictions are in closer agreement (Fig. 6c), except near both edges. The drag integrated from the wall stress distribution differs by only 5% at this Reynolds number. As might be expected, the local shear stresses at both the leading and trailing edge are not well predicted by boundary layer theory even for higher Reynolds numbers. The approximation over-predicts near the leading edge, predicting an infinite shear stress at the singular point $x = 0$. The difference at the trailing edge is also very large, amounting to a 49% error for $Re = 86.5$ and $n = 0.28$. Similar behaviour is also found to exist for other values of n.

As a useful guide for practical applications, a 5% error limit is chosen as the criterion to select the minimum Reynolds number for the applicability of boundary layer theory. At lower Reynolds numbers the boundary layer approximation is considered to be inadequate. The results for a range of shear-thinning index n are given in Table 2.

4.3. *Influence of angle of attack*

Typical experimental results are shown in Fig. 7a at three Reynolds numbers for $\alpha = 0$–$90°$. The drag is the largest when the plate is normal to the flow and smallest when it is tangential to the flow. The details of the variation of C_D with the angle of attack can be approximated by the model curves shown in the figures. The curves represent the model equation developed in Section 3.1; the non-dimensional form of Eq. (5) is expressed in the following way:

$$C_D = C_{Dn} \sin^2 \alpha + C_{Dt} \cos^2 \alpha. \tag{9}$$

Where C_{Dn} and C_{Dt} are drag coefficients for the plate placed normal and tangential to the flow, respectively. The agreement between the creeping model predictions and the experimental results is good even outside the creeping flow region as shown in Fig. 7a, suggesting that non-linearities due to flow inertia and shear-thinning characteristics do not have a substantial influence on modifying the variation of drag with angle of attack, at least for the Reynolds number range investigated. The use of the present model offers a simple way to estimate the drag force of a plate placed at an arbitrary angle to the flow, provided that both the drags of the plate aligned at 0° and 90° to the flow are known or can be determined.

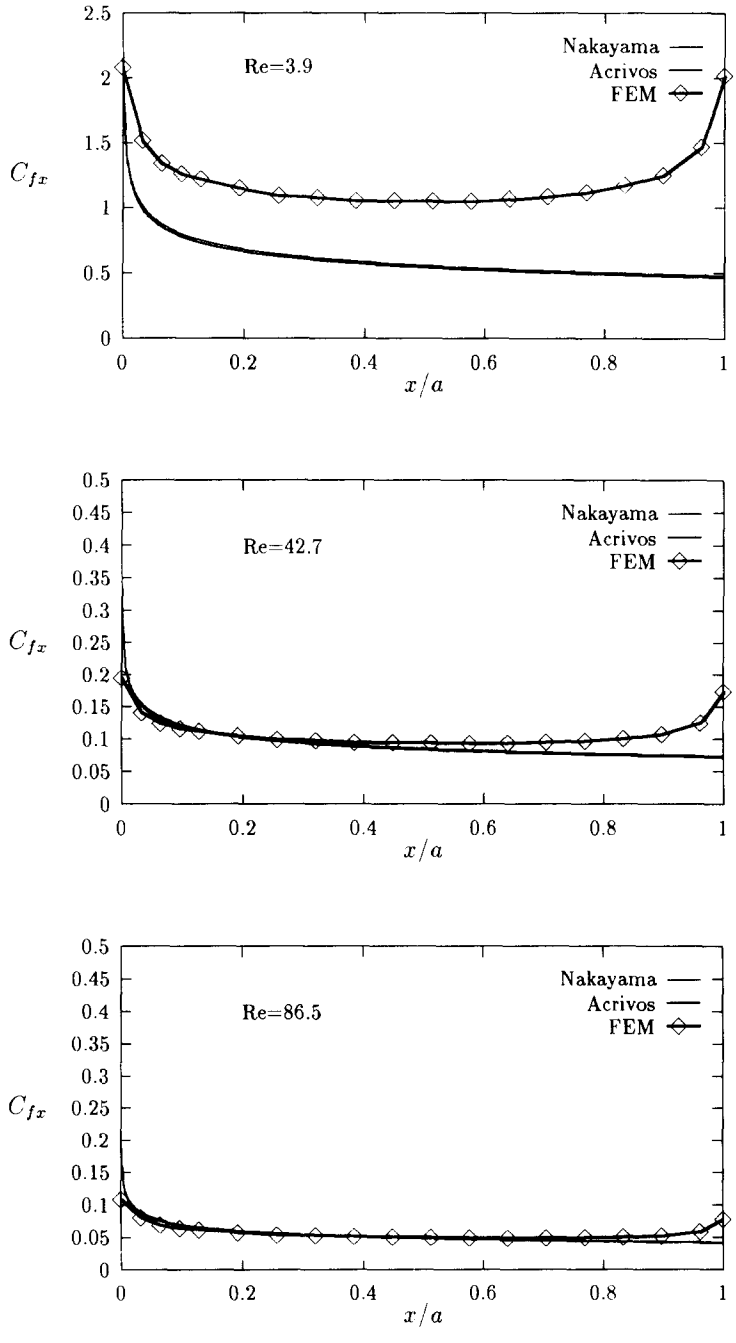

Fig. 6. Local skin friction $C_{fx} = \tau_0/1/2\rho U^2$ distribution along the plate: the points are the FEM simulation and the lines are the boundary layer theory prediction. The power-law index is $n = 0.28$ (a) Re = 3.9; (b) Re = 42.7; (c) Re = 86.7.

Table 2
Suggested minimum Reynolds numbers for the applicability of the boundary layer approximation for non-Newtonian shear-thinning fluid flows (at the listed Reynolds numbers the error in the estimated integrated drag is about 5%)

n	0.1	0.32	0.60	0.80	1.0
Re	45	100	200	170	120

The influence of non-Newtonian shear-thinning was determined by varying n in the FEM code and computing drags at various α. Typical results are plotted in Fig. 7b. The curves in the figure are predictions using the superposition model. It is interesting that at small angles of attack, the drag coefficient reduces as the shear-thinning effect increases, whereas at large angles of attack, the drag coefficient increases as the shear-thinning effect reduces.

This indicates that there is a critical angle below which shear-thinning causes drag reduction and above which non-Newtonian shear-thinning causes drag augmentation. This will be discussed in more detail in the following section.

4.4. Drag on a flat plate normal to the flow

Fig. 8 plots the results for the drag coefficient variation with the generalized Reynolds number for a number of different shear-thinning indices n. It is noted that, at a given Reynolds number, the drag coefficient of a plate normal to the flow increases for increasing shear-thinning as n is reduced. This trend is exactly opposite to that of the plate placed tangentially to the flow. Instead of drag reduction, drag augmentation is then observed. This can be explained through the following argument. The drag consists of two components, i.e. skin friction drag due to wall shear stress and form drag due to pressure difference. These two components can vary with shear-thinning in different ways. Since drag of a flat plate placed normally to the flow is solely determined by form drag, this implies that pressure induced drag increases with shear-thinning. In a similar way, it is clear that since the drag of a flat plate placed tangentially to the flow is solely due to wall shear stress, it is apparent that skin friction reduces as shear-thinning increases. For a plate placed at an arbitrary angle of attack, both components contribute and a critical angle separates the region into two zones. The effect of increasing non-Newtonian shear-thinning can be summarized as follows: at angles smaller than the critical angle, wall shear stress is dominant leading to drag reduction, and at angles larger than the critical angle, surface pressure is dominant resulting in drag augmentation.

It is also interesting that the curves of the normal drag coefficient vs. Reynolds number are straight lines at low Reynolds numbers (typically for $\mathrm{Re} < 4$) and become non-linear at higher Reynolds numbers ($\mathrm{Re} \geq 4$). This is associated with a transition from the creeping flow region to an inertial region at higher Reynolds numbers. This change is delayed when the plate is placed tangentially to the flow, as is evident from Fig. 5, where it is seen that the drag coefficient curves are straight lines even for $\mathrm{Re} > 100$.

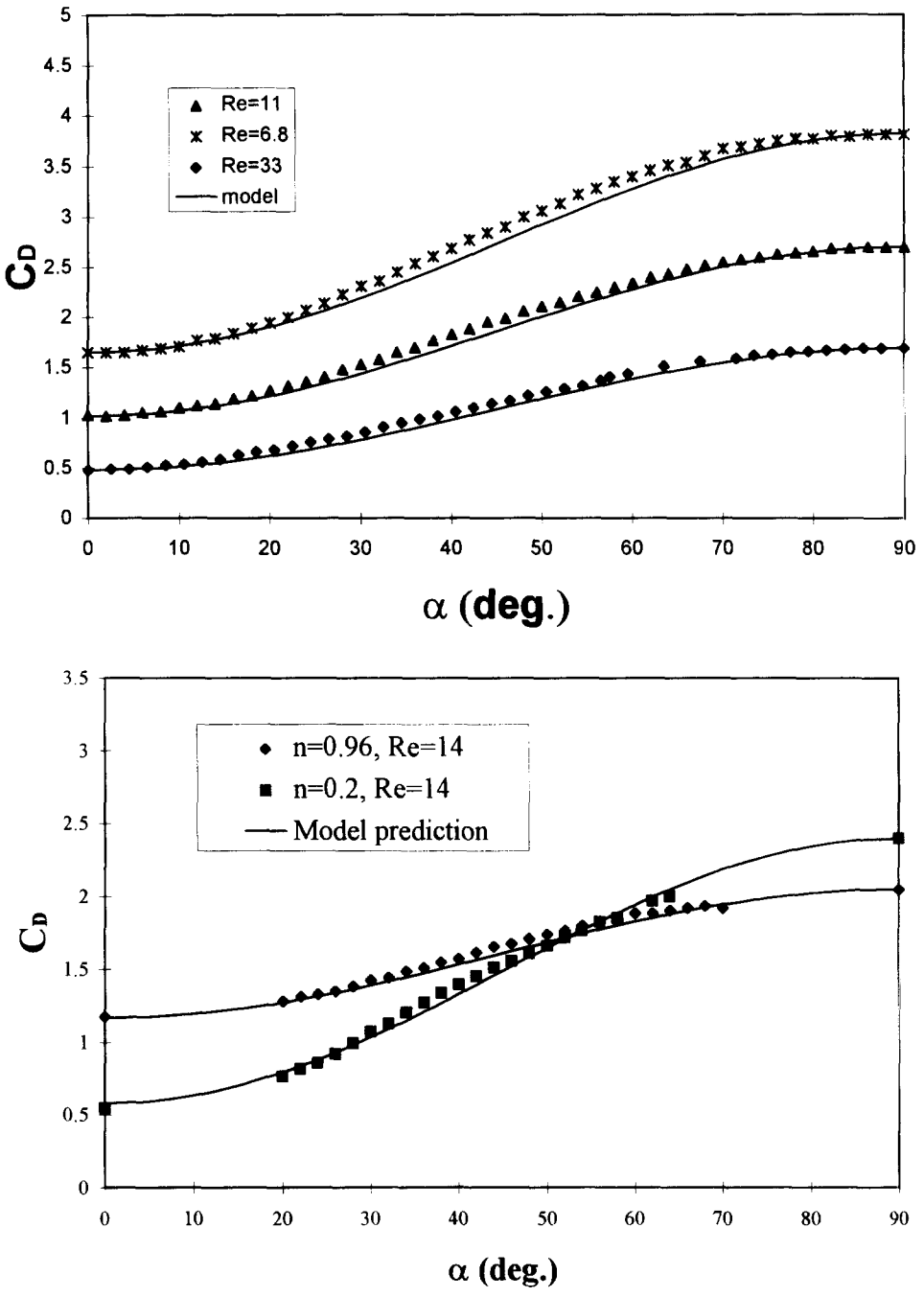

Fig. 7. Drag of flat plate placed at arbitrary angle of attack. (a) Reynolds number effect: points are experimental, lines are application of the superposition model. The shear-thinning index is $n = 0.32$. (b) Shear-thinning effect, $\mathrm{Re} = 14$. The points are from FEM simulations.

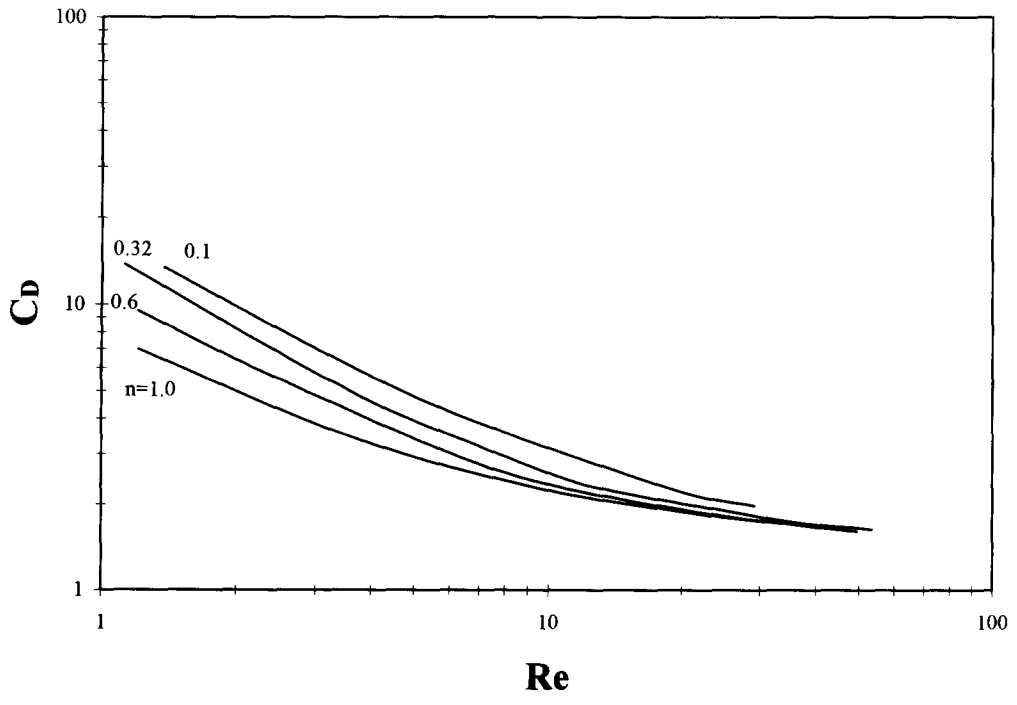

Fig. 8. Drag coefficient for a flat plate aligned normally to a (non-Newtonian) flow.

4.5. *Lift of a flat plate*

One important feature of flow past an inclined flat plate is the development of a force normal to the flow, i.e. lift. An equivalent form of Eq. (9) for lift coefficient can also be derived for creeping flow:

$$C_L = \tfrac{1}{2}(C_{Dn} - C_{Dt}) \sin 2\alpha. \tag{10}$$

To examine the applicability and generality of this equation in the creeping flow regime, the lift coefficient at $\alpha = 45$ was computed and compared with $(C_{Dn} - C_{Dt})/2$ in Fig. 9 for Re = 0.06 and over a range of n. Good agreement between the two is apparent. This result suggests that the non-linearity due to shear-thinning is not important in the creeping flow regime and the simple superposition model is valid for both Newtonian and non-Newtonian flows.

It is also noted that, at a given generalized Reynolds number, the lift coefficient increases as shear-thinning increases. This is largely due to the fact that an increase in shear-thinning causes an increase in the drag coefficient of the plate placed normal to flow in the creeping flow regime.

It is of interest to characterize the angle at which maximum lift occurs. The linear model predicts that this angle should be 45° for creeping flow, as is clearly implied by Eq. (10). In et al. [10] showed that for Newtonian flow this angle is equal to 45° at Re = 1 and decreases as the Reynolds number increases. Fig. 10 summarizes the present results for different shear-thinning indices and the Newtonian results of In et al. The data for both Newtonian and non-Newtonian fluids appears to collapse into a single curve, suggesting that non-Newtonian effect may not be crucial in determining the angle at which maximum lift occurs.

This is further confirmed by the results shown in Fig. 11, where the lift coefficients at Re = 14 for two different shear-thinning indices are plotted against the angle of attack. The maxima for both curves occur for $\alpha \approx 35°$, despite the difference in the value of n. The deviation from the theoretical prediction of 45° is related to the effect of inertia, which at higher Reynolds numbers contributes to the formation of a dead zone behind the plate with vortices either attaching to or shedding from the plate, causing a reduction in lift. The other interesting feature borne out by Fig. 11, as mentioned previously, is that C_L increases as n decreases, suggesting that non-Newtonian shear-thinning increases the lift coefficient.

Eq. (10) indicates that the lift coefficient is proportional to the difference between the two drag coefficients of the plate, placed normally and tangentially to the flow. Since the former increases with shear-thinning and the latter reduces with shear-thinning, it is clear that the result shown in Fig. 11 is qualitatively in agreement with the trend predicted by the linear model developed for creeping flow.

5. Discussion

Adachi et al. [1] solved for the flow of non-Newtonian shear-thinning fluids past a sphere numerically. They decomposed the total drag of the sphere into friction drag and pressure drag, and found that the friction drag decreases and the pressure drag increases, as shear-thinning

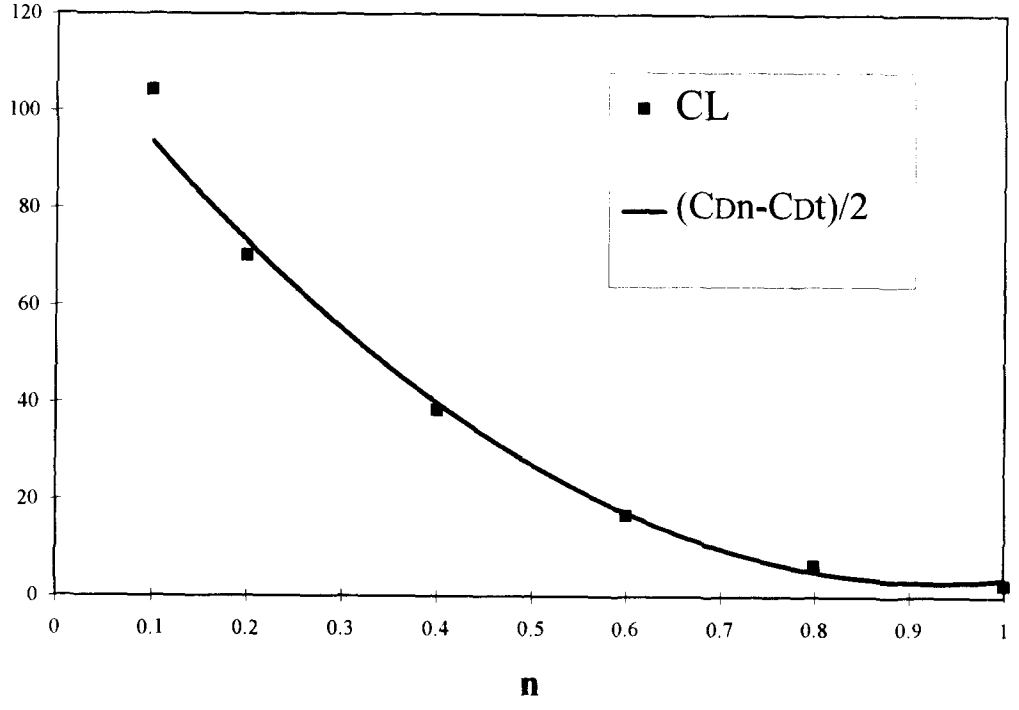

Fig. 9. Comparison between lift coefficient at $\alpha = 45°$ and $\frac{1}{2}(C_{Dn} - C_{Dt})$: variation with shear-thinning index n for creeping flow, Re = 0.06.

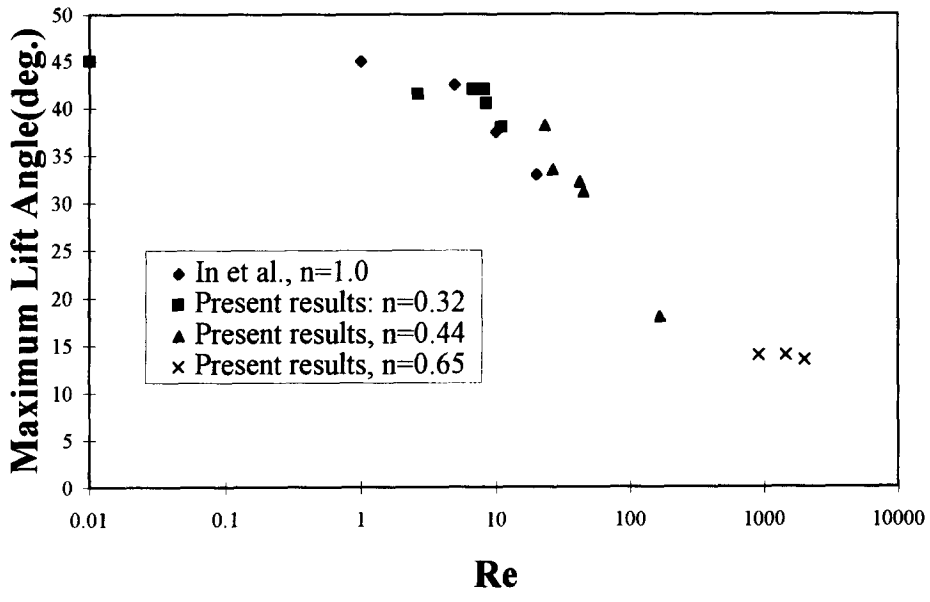

Fig. 10. Maximum lift angle variation with Reynolds number, numerical and experimental results.

increases. Similar behaviour was found in the present work. The ratio of pressure drag to friction drag is crucial in determining the effect of non-Newtonian shear-thinning on the total drag of a body. For a flat plate, this ratio is dependent on the angle of attack, as demonstrated in the present work. The magnitude of this influence is dependent on the Reynolds number. For instance, in the low Reynolds number range, the non-Newtonian effect becomes marginal in modifying the drag of a plate placed tangentially to the flow, as is evident in Fig. 5.

The linear model developed in this work may serve as a useful tool in quickly determining the drag coefficient of a flat plate at an arbitrary angle for both Newtonian and non-Newtonian fluid flows, provided that the two drag coefficients for the plate, i.e. for the plate placed normally and tangentially to the flow, are known. This appears to indicate that the non-linearity caused by both inertia and shear-thinning does not influence the variation of drag with the angle of attack substantially, although these two drag coefficients are influenced by both inertia and shear-thinning. It seems likely that this estimation method may also be useful for more general geometries, such as airfoil-shaped bodies. Future work is needed to verify this conjecture.

6. Conclusions

The lift and drag coefficients of a flat plate placed in a power-law non-Newtonian fluid have been investigated both experimentally and numerically. Simulations using a FEM code predict lift and drag coefficients in good agreement with experimental results obtained with a force balance. A linear Newtonian creeping flow model was described which uses the drag coefficients for the plate at 0° and 90° to the flow to predict drag and lift at intermediate angles. The results show that the model works well even outside the creeping flow region.

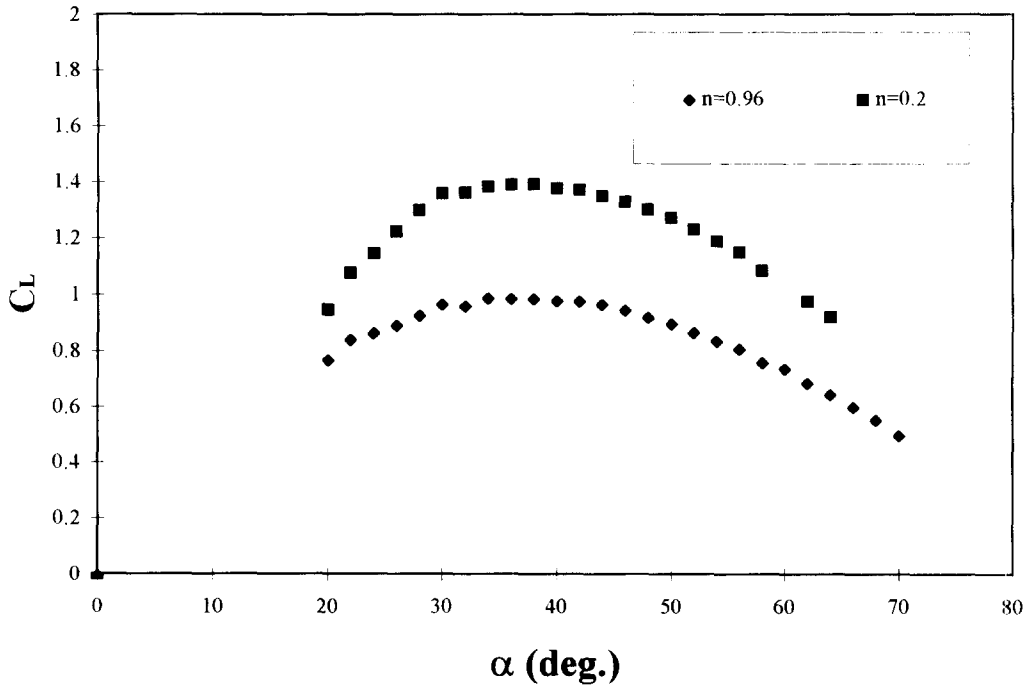

Fig. 11. Lift coefficient variation with angle of attack of the plate at Re = 14, $n = 0.2$ and 1.0.

Shear-thinning was found to cause drag reduction for a flat plate at small angles of attack and drag augmentation at large angles of attack. In addition, the lift coefficient increases as shear-thinning is increased. This result is also consistent with the linear theory. The angle at which the maximum lift occurs is not sensitive to non-Newtonian shear-thinning; this angle decreases from the theoretical value of 45° in the creeping flow regime to smaller values at higher Reynolds numbers.

The present study also determined the extent of the applicability of the boundary layer approximation for a flat plate placed tangentially to the flow. Minimum Reynolds numbers have been provided for a range of shear-thinning index n for which the boundary layer approximation (for drag), gives at most 5% integrated error.

Acknowledgements

The authors thank Dr. Y. Li, M.C. Welsh and Dr. L. Pullum for many helpful discussions.

References

[1] K. Adachi, N. Yoshioka and K. Yamamoto, On non-Newtonian flow past a sphere, Chem. Eng. Sci., 28 (1973) 2033.

[2] K. Adachi, N. Yoshioka and K. Sakai, An investigation of non-Newtonian flow past a sphere, J. Non-Newtonian Fluid Mech., 3 (1977–78) 107–125.
[3] G.U. Dazhia and R.I. Tanner, The drag on a sphere in a power-law fluid, J. Non-Newtonian Fluid Mech., 17 (1985) 1–12.
[4] B. Mena and O. Manero, The influence of rheological properties on the slow flow past spheres, J. Non-Newtonian Fluid Mech., 26 (1987) 247–275.
[5] R.P. Chhabra, Hydrodynamics of bubbles and drops in rheologically complex liquids, in N.P. Cheremisinoff (Ed.), Encyclopedia of Fluid Mechanics, Vol. 7, Rheology and Non-Newtonian Flows, Gulf Publishing Co., Houston, 1986, pp. 253–286.
[6] W.R. Schowalter, The application of boundary-layer theory to power-law pseudo-plastic fluids: similar solutions, AICHE J., 6 (1960) 24–28.
[7] A. Acrivos, M.J. Shah and E.E., Petersen, Momentum and heat transfer in laminar boundary-layer flows of non-newtonian fluids past external surfaces, AICHE J., 6 (1960) 312–317.
[8] A. Nakayama, Integral method for forced convection heat transfer in power-law non-newtonian fluids, in N.P. Cheremisinoff (Ed.), Encyclopedia of Fluid Mechanics, Vol. 7, Rheology and Non-Newtonian Flows, Ch. 2. Gulf Publishing Co., Houston, 1986.
[9] H.I. Andersson and T.H. Toften, Numerical solution of the laminar boundary layer equations for power-law fluids, J. Non-Newtonian Fluid Mech., 32 (1989) 175–195.
[10] K.M. In, D.H. Choi, and M.-U. Kim, Two-dimensional viscous flow past a flat plate, Fluid Dyn. Res., 15 (1995) 13–24.
[11] K. Tamada, H. Miura and T. Miyagi, Low-Reynolds-number flow past a cylindrical body, J. Fluid Mech., 132 (1983) 445–455.
[12] O.C. Zienkiewicz and R.L. Taylor, The Finite-Element Method, McGraw-Hill, London 4th edn., 1989.
[13] L. Rubart and G. Böhme, Numerical simulation of shear thinning flow problems in mixing vessels, Theor. Comput. Fluid Dyn., 3 (1991) 95–115.